Reflection and transmission of Lamb waves at an imperfect joint of plates

Cite as: J. Appl. Phys. **113**, 074901 (2013); https://doi.org/10.1063/1.4791711
Submitted: 26 December 2012 • Accepted: 28 January 2013 • Published Online: 15 February 2013

Naoki Mori, Shiro Biwa and Takahiro Hayashi

Reflection and transmission of Lamb waves at an imperfect joint of plates

Naoki Mori, Shiro Biwa,[a] and Takahiro Hayashi
Department of Aeronautics and Astronautics, Graduate School of Engineering, Kyoto University, Kyoto 615-8540, Japan

(Received 26 December 2012; accepted 28 January 2013; published online 15 February 2013)

The reflection and transmission of Lamb waves at an imperfect joint of plates are analyzed numerically by the modal decomposition method and the hybrid finite element method. The joint is modeled as a spring-type interface characterized by distributed normal and tangential stiffnesses. The analysis is focused on a low-frequency range where the lowest-order symmetric and antisymmetric Lamb waves are the only propagating modes. The frequency-dependent reflection and transmission characteristics of these Lamb modes are computed for different interfacial stiffnesses, together with the generation behavior of localized, non-propagating higher-order Lamb modes. As a result, S0-mode Lamb wave is shown to exhibit the reflection and transmission characteristics which are monotonically frequency-dependent. On the other hand, A0-mode Lamb wave shows complicated and non-monotonic frequency dependence in the reflection and transmission characteristics. The obtained Lamb wave characteristics are discussed in the light of approximate one-dimensional models constructed based on classical plate theories. As a result, the reflection and transmission coefficients of S0-mode Lamb wave are accurately reproduced by a simple model of longitudinal wave in thin plates, while those of A0-mode Lamb wave are well described by the Mindlin plate model of flexural wave. It is also shown that stiffness reduction at the corners of the contacting edges of plates has only minor influence on the reflection and transmission characteristics. © *2013 American Institute of Physics*.
[http://dx.doi.org/10.1063/1.4791711]

I. INTRODUCTION

Ultrasonic waves offer an efficient nondestructive means to evaluate crack-type defects in structural components. When such defects undergo partial closure due to compressive stresses or temperature variation, however, ultrasonic waves exhibit partial reflection and transmission at their contacting faces, which can complicate the evaluation procedure.[1] Understanding interaction of ultrasonic waves with contacting surfaces is thus an important issue to fully interpret the acquired experimental data.

Contacting surfaces are often modeled as spring-type interfaces which have finite normal and tangential stiffnesses.[2,3] This spring-interface model can not only describe linear acoustic properties of contacting surfaces but also be extended to analyze their nonlinear properties.[4–7] This model also applies reasonably well to other types of imperfect interfaces such as a damaged interface[8] and a thin layer between solids.[9] Interactions of ultrasonic waves with spring-type interfaces in structural components have been studied by many investigators, including the wave propagation across multiple spring-type interfaces[10,11] as well as along a spring-type interface.[12–17] Li and Achenbach[18] studied Rayleigh wave scattering at a spring-type interface, and Pecorari[19] analyzed Rayleigh wave scattering by a partially closed surface-breaking crack.

Corresponding issues of the Lamb wave reflection and transmission at contacting edges of plates are not only of academic interest but also relevant to ultrasonic monitoring of, e.g., closed fatigue cracks in plate-like structures which has been a topic of recent investigation.[20,21] In literature, interactions of Lamb waves with local discontinuities have been studied extensively. Investigations reported so far include Lamb wave interaction with free and fixed edges[22–25] and various types of defects.[26–34] Lamb wave transmission through a strip weld has been analyzed by Al-Nassar *et al.*[35] and Predoi and Rousseau.[36] To the best of the present authors' knowledge, however, the corresponding issue for a spring-type joint of plates has not been explored in the foregoing literature in spite of its importance in clarifying the physical background to evaluate closed defects in thin-walled structures.

The aim of the present study is thus to elucidate the fundamental characteristics of reflection and transmission of Lamb waves at a spring-type joint of plates, by numerical analysis based on the modal decomposition method (MDM)[30,33] and the hybrid finite element method (HFEM).[35,37] The analysis is focused on a low-frequency range where the lowest-order symmetric and antisymmetric Lamb waves are the only propagating modes. The frequency-dependent reflection and transmission characteristics of these Lamb modes are computed for different interfacial stiffnesses, together with the generation behavior of localized, non-propagating higher-order Lamb modes. In order to interpret the underlying physical phenomena, classical plate theories are employed to construct one-dimensional models for longitudinal and flexural waves in thin jointed plates. Furthermore, the influence of stiffness reduction at the corners of the contacting edges on the reflection and transmission characteristics is also examined.

[a]Author to whom correspondence should be addressed. Electronic mail: biwa@kuaero.kyoto-u.ac.jp.

II. ANALYSIS

A. Governing equations

As shown in Fig. 1, two semi-infinite plates of thickness d are in partial contact with each other at $x = 0$ in the x-z coordinate system. The contacting edges of plates constitute an imperfect joint, which is modeled as a spring-type interface characterized by distributed normal and tangential stiffnesses K_N and K_T, respectively. The two plates are made of the same isotropic and linear elastic solid with density ρ and Lamé's constants λ and μ. The interaction of Lamb waves with the interface is analyzed presently in the frequency domain, where the angular frequency is denoted by ω. The displacement components in the plates in the x and z directions are denoted by $u(x, z)$ and $w(x, z)$, respectively.

In the frequency domain, the displacement components obey

$$\begin{aligned}(\lambda+\mu)\frac{\partial}{\partial x}\left(\frac{\partial u}{\partial x}+\frac{\partial w}{\partial z}\right)+\mu\left(\frac{\partial^2}{\partial x^2}+\frac{\partial^2}{\partial z^2}\right)u+\rho\omega^2 u=0,\\ (\lambda+\mu)\frac{\partial}{\partial z}\left(\frac{\partial u}{\partial x}+\frac{\partial w}{\partial z}\right)+\mu\left(\frac{\partial^2}{\partial x^2}+\frac{\partial^2}{\partial z^2}\right)w+\rho\omega^2 w=0,\end{aligned} \tag{1}$$

in the absence of body forces. The upper and lower surfaces of the plates ($z = \pm d/2$) are assumed to be traction-free. The boundary conditions at $x = 0$ are given by

$$\sigma(0^-, z) = \sigma(0^+, z) = K_N[u(0^+, z) - u(0^-, z)], \tag{2a}$$

$$\tau(0^-, z) = \tau(0^+, z) = K_T[w(0^+, z) - w(0^-, z)], \tag{2b}$$

where σ ($=\sigma_{xx}$) is the normal stress in the x direction and τ ($=\sigma_{xz}$) the shear stress: the superimposed plus (minus) denotes the limit from the positive (negative) side of the interface. The stiffnesses K_N and K_T can be functions of z.

The wave fields in a plate satisfying the traction-free surface conditions are known as Lamb modes, which are composed of symmetric (S) and antisymmetric (A) modes. For a given angular frequency ω, there are an infinite number of (real, imaginary or complex) wave number k satisfying the dispersion relations (Rayleigh-Lamb frequency equations[38]), each k giving a particular Lamb mode.

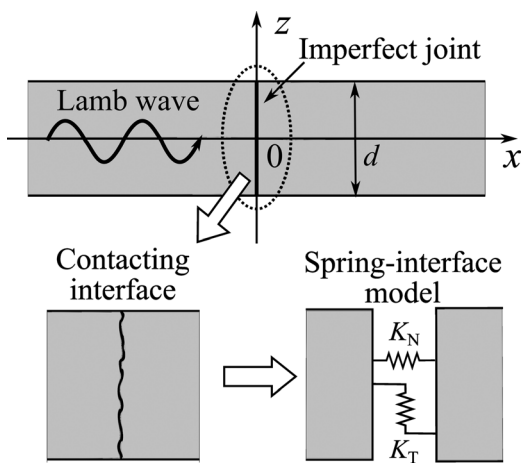

FIG. 1. Two plates jointed by a spring-type interface.

For an nth-order symmetric Lamb mode (distinguished by a superscript S), the displacement and stress components are expressed as

$$\begin{aligned}u^S_{\pm n}(x, z) &= U^S(z; k^S_{\pm n})\exp(\mathrm{i}k^S_{\pm n}x),\\ w^S_{\pm n}(x, z) &= W^S(z; k^S_{\pm n})\exp(\mathrm{i}k^S_{\pm n}x),\end{aligned} \tag{3a}$$

$$\begin{aligned}\sigma^S_{\pm n}(x, z) &= \Sigma^S(z; k^S_{\pm n})\exp(\mathrm{i}k^S_{\pm n}x),\\ \tau^S_{\pm n}(x, z) &= \mathrm{T}^S(z; k^S_{\pm n})\exp(\mathrm{i}k^S_{\pm n}x),\end{aligned} \tag{3b}$$

where $k^S_{\pm n}$ ($n = 0, 1, 2,\ldots$) are the wave numbers for the symmetric mode, the subscript $+$ ($-$) corresponding to the Lamb modes which are propagating (for real wave numbers) or decaying (for complex wave numbers) in the positive (negative) x-direction. The cross-sectional profiles are given by $U^S(z; k^S_{\pm n})$, $W^S(z; k^S_{\pm n})$, $\Sigma^S(z; k^S_{\pm n})$, and $\mathrm{T}^S(z; k^S_{\pm n})$: their explicit forms can be found elsewhere.[35–38]

Likewise, for an nth-order antisymmetric Lamb mode (distinguished by a superscript A), the displacement and stress components are written as

$$\begin{aligned}u^A_{\pm n}(x, z) &= U^A(z; k^A_{\pm n})\exp(\mathrm{i}k^A_{\pm n}x),\\ w^A_{\pm n}(x, z) &= W^A(z; k^A_{\pm n})\exp(\mathrm{i}k^A_{\pm n}x),\end{aligned} \tag{4a}$$

$$\begin{aligned}\sigma^A_{\pm n}(x, z) &= \Sigma^A(z; k^A_{\pm n})\exp(\mathrm{i}k^A_{\pm n}x),\\ \tau^A_{\pm n}(x, z) &= \mathrm{T}^A(z; k^A_{\pm n})\exp(\mathrm{i}k^A_{\pm n}x).\end{aligned} \tag{4b}$$

In the present analysis, the functions $U^\alpha(z; k^\alpha_{\pm n})$, $W^\alpha(z; k^\alpha_{\pm n})$, $\Sigma^\alpha(z; k^\alpha_{\pm n})$, and $\mathrm{T}^\alpha(z; k^\alpha_{\pm n})$ ($\alpha = \mathrm{S}$ or A) are assumed to be normalized in the sense that the following relation holds,[31] i.e.:

$$\begin{aligned}\frac{\mathrm{i}\omega}{4}\int_{-d/2}^{d/2}\{[U^\alpha(z; k^\alpha_{\pm n})\Sigma^{\alpha*}(z; k^{\alpha*}_{\pm n}) + V^\alpha(z; k^\alpha_{\pm n})\mathrm{T}^{\alpha*}(z; k^{\alpha*}_{\pm n})]\\ -[U^{\alpha*}(z; k^{\alpha*}_{\pm n})\Sigma^\alpha(z; k^\alpha_{\pm n}) + V^{\alpha*}(z; k^{\alpha*}_{\pm n})\mathrm{T}^\alpha(z; k^\alpha_{\pm n})]\}dz = \pm 1.\end{aligned} \tag{5}$$

In the above expressions, the superscript * indicates complex conjugate. Namely, $U^{\alpha*}(z; k^{\alpha*}_{\pm n})$, $W^{\alpha*}(z; k^{\alpha*}_{\pm n})$, $\Sigma^{\alpha*}(z; k^{\alpha*}_{\pm n})$, and $\mathrm{T}^{\alpha*}(z; k^{\alpha*}_{\pm n})$ are the complex conjugates of the modal functions $U^\alpha(z; k^{\alpha*}_{\pm n})$, $W^\alpha(z; k^{\alpha*}_{\pm n})$, $\Sigma^\alpha(z; k^{\alpha*}_{\pm n})$, and $\mathrm{T}^\alpha(z; k^{\alpha*}_{\pm n})$, respectively, for the Lamb mode which has the wave number $k^{\alpha*}_{\pm n}$ complex conjugate to $k^\alpha_{\pm n}$ (conjugate non-propagating mode[31]). For propagating modes with real wave numbers, $k^\alpha_{\pm n} = k^{\alpha*}_{\pm n}$, Eq. (5) reduces to the statement that their time-averaged power is unity.

A lowest-order symmetric (S0) mode or a lowest-order antisymmetric (A0) mode, propagating in the positive x direction, is considered as the incident field. The incident Lamb mode interacts with the spring-type interface and gives rise to both transmitted and reflected wave fields. It is assumed that the frequency $f = \omega/(2\pi)$ of the incident Lamb mode is below the first cut-off frequency,

$$f_{A1} = \frac{c_T}{2d}, \tag{6}$$

where c_T is the transverse wave velocity. Below this frequency, S0 and A0 are the only propagating Lamb modes

with real wave numbers. Therefore, sufficiently away from the interface, the transmitted and reflected fields essentially contain S0 and A0 modes only.

B. Modal decomposition method

The wave field in a plate can be expressed in the form of normal mode expansion,[39] i.e., as linear combinations of Lamb modes of different orders. When a Lamb mode propagating in the positive x-direction is incident to the interface at $x=0$, the wave field in the left plate is given by the sum of the incident Lamb mode and the Lamb modes generated at the interface (referred to as reflected Lamb modes, including non-propagating modes). With the notations given above, the displacements are expressed as

$$u = U^{\alpha}(z;k^{\alpha}_{+0})\exp(\mathrm{i}k^{\alpha}_{+0}x) + \sum_{n=0}^{\infty} R_{\mathrm{S}n}U^{\mathrm{S}}(z;k^{\mathrm{S}}_{-n})\exp(\mathrm{i}k^{\mathrm{S}}_{-n}x) + \sum_{n=0}^{\infty} R_{\mathrm{A}n}U^{\mathrm{A}}(z;k^{\mathrm{A}}_{-n})\exp(\mathrm{i}k^{\mathrm{A}}_{-n}x), \tag{7a}$$

$$w = W^{\alpha}(z;k^{\alpha}_{+0})\exp(\mathrm{i}k^{\alpha}_{+0}x) + \sum_{n=0}^{\infty} R_{\mathrm{S}n}W^{\mathrm{S}}(z;k^{\mathrm{S}}_{-n})\exp(\mathrm{i}k^{\mathrm{S}}_{-n}x) + \sum_{n=0}^{\infty} R_{\mathrm{A}n}W^{\mathrm{A}}(z;k^{\mathrm{A}}_{-n})\exp(\mathrm{i}k^{\mathrm{A}}_{-n}x), \tag{7b}$$

for $x<0$, where $R_{\mathrm{S}n}$ ($R_{\mathrm{A}n}$) gives the coefficient of the reflected Sn mode (An mode). The incident Lamb mode, with $\alpha=$ S (A) for S0 mode (A0 mode), has unit time-averaged power according to Eq. (5).

For the right plate ($x>0$), the wave field (consisting of transmitted Lamb modes) is given by

$$u = \sum_{n=0}^{\infty} T_{\mathrm{S}n}U^{\mathrm{S}}(z;k^{\mathrm{S}}_{+n})\exp(\mathrm{i}k^{\mathrm{S}}_{+n}x) + \sum_{n=0}^{\infty} T_{\mathrm{A}n}U^{\mathrm{A}}(z;k^{\mathrm{A}}_{+n})\exp(\mathrm{i}k^{\mathrm{A}}_{+n}x), \tag{8a}$$

$$w = \sum_{n=0}^{\infty} T_{\mathrm{S}n}W^{\mathrm{S}}(z;k^{\mathrm{S}}_{+n})\exp(\mathrm{i}k^{\mathrm{S}}_{+n}x) + \sum_{n=0}^{\infty} T_{\mathrm{A}n}W^{\mathrm{A}}(z;k^{\mathrm{A}}_{+n})\exp(\mathrm{i}k^{\mathrm{A}}_{+n}x), \tag{8b}$$

where $T_{\mathrm{S}n}$ ($T_{\mathrm{A}n}$) is the coefficient of the transmitted Sn mode (An mode).

For each plate, the stress fields can be expressed likewise in terms of the functions $\Sigma^{\alpha}(z;k^{\alpha}_{\pm n})$ and $\mathrm{T}^{\alpha}(z;k^{\alpha}_{\pm n})$ ($\alpha=$ S or A) defined in Eqs. (3) and (4). Then, substituting these modal expansion expressions into Eqs. (2a) and (2b), the boundary conditions are written in terms of the known modal functions $U^{\alpha}(z;k^{\alpha}_{\pm n})$, $W^{\alpha}(z;k^{\alpha}_{\pm n})$, $\Sigma^{\alpha}(z;k^{\alpha}_{\pm n})$, $\mathrm{T}^{\alpha}(z;k^{\alpha}_{\pm n})$ ($\alpha=$ S or A) and the unknown modal coefficients $R_{\mathrm{S}n}$, $T_{\mathrm{S}n}$, $R_{\mathrm{A}n}$, $T_{\mathrm{A}n}$ ($n=0, 1, 2,\ldots$).

In the modal decomposition method (MDM),[30,33] the infinite series in the above expressions is replaced by finite ones by truncating them at finite n, i.e., at $n=n_{\mathrm{S}}$ for S modes and $n=n_{\mathrm{A}}$ for A modes. Then, there are $n_{\mathrm{X}}=2(n_{\mathrm{S}}+n_{\mathrm{A}}+2)$ unknown coefficients, consisting of $R_{\mathrm{S}n}$ and $T_{\mathrm{S}n}$ for $n=0, 1, 2,\ldots, n_{\mathrm{S}}$, and $R_{\mathrm{A}n}$ and $T_{\mathrm{A}n}$ for $n=0, 1, 2,\ldots, n_{\mathrm{A}}$. To solve for these coefficients, the boundary conditions are evaluated at n_{C} collocation points in $-d/2<z<d/2$, resulting in a set of $4n_{\mathrm{C}}$ linear equations with complex coefficients. When $4n_{\mathrm{C}}>n_{\mathrm{X}}$, the reflection and transmission coefficients can be obtained numerically as a least-square-norm solution to this set of equations by the singular value decomposition (SVD) procedure. The number of Lamb modes to be accounted for needs to be determined in the numerical analysis to acquire accuracy of a sufficient level. The energy conservation principle can be employed to validate the accuracy of numerical solutions. Since only the lowest-order modes carry energy away from the interface in the frequency range considered, the quantity defined by

$$\delta = \left| 1 - \sum_{\alpha=\mathrm{S,A}} \left(|R_{\alpha 0}|^2 + |T_{\alpha 0}|^2 \right) \right| \tag{9}$$

should be zero because of the normalization given in Eq. (5). Therefore, the value of δ is used as a measure of numerical accuracy of the solution obtained.

C. Hybrid finite element method

Although MDM has been successfully employed for the study of Lamb wave scattering by a crack[30] and a rectangular notch,[33] the convergence of the modal expansion may deteriorate when the problem to be analyzed contains a stress singularity.[23] Such singularity can be present at the corners of the contacting edges of plates ($x=0$ and $z=\pm d/2$) in the present analysis. Therefore, in order to partly verify the numerical solutions obtained by MDM, the hybrid finite element method (HFEM)[35,37] is employed as an alternative approach to analyze the Lamb wave reflection and transmission at the spring-type interface. In this method, a region surrounding the interface is divided into finite elements and the wave field therein is expressed in terms of nodal displacements. In the outer semi-infinite regions, the wave fields are expressed as combination of different Lamb modes as in MDM. The continuity of the displacements and tractions is applied at the boundaries between the finite element region and the outer regions. As a result, a set of equations can be constructed to determine the nodal displacements in the finite-element region and the coefficients of the Lamb-wave modal expansion. The above-mentioned SVD method is used to determine the nodal displacements and the outer-region Lamb mode coefficients numerically.

In the present analysis, a rectangular region of length L, $-L/2<x<L/2$, is divided into finite elements, and the Lamb-wave modal expansion is adopted for semi-infinite regions $x<-L/2$ and $x>L/2$. The length L then becomes a key parameter in the numerical analysis. Higher-order Lamb modes decay faster as one moves away from the interface. A longer L allows the outer fields to be represented by a smaller number of Lamb modes within a numerical tolerance, while it requires a greater number of finite elements to be employed for the inner region.

III. NUMERICAL RESULTS

A. Setting of numerical parameters

Numerical analysis has been performed for the S0 (or A0) incident Lamb mode in the normalized frequency range $0 < fd/c_T < 0.5$ given by Eq. (6). For 1-mm-thick aluminum plates ($\rho = 2700\,\mathrm{kg\ m^{-3}}$, $\lambda = 56.3\,\mathrm{GPa}$, $\mu = 27.1\,\mathrm{GPa}$), this corresponds to $0 < f < f_{A1} = 1.585\,\mathrm{MHz}$. Poisson's ratio of the plates is set as $\nu = \lambda/\{2(\lambda+\mu)\} \cong 0.34$. Different values of interfacial stiffnesses are considered in normalized forms $K_N\, d/\mu$ and $K_T\, d/\mu$. Unless otherwise stated, the interfacial stiffnesses are assumed to be independent of z: Effects of their distribution are considered later in Sec. IV C where they are assumed symmetric functions of z.

In the above frequency range, the computation with MDM required 14 symmetric and antisymmetric modes to be taken into account ($n_S = n_A = 13$) to keep δ below 0.1% for the S0-mode incidence and below 0.5% for the A0-mode incidence, when 15 collocation points ($n_C = 15$) were arranged at

$$z_j = -\frac{d}{2} + \frac{d}{1+n_C} j \quad (j = 1, 2, \ldots, n_C). \tag{10}$$

For the analysis with HFEM, the length of the inner finite-element region was set as $L = d/2$, and 200 square-shaped, four-noded isoparametric finite elements of dimensions $d/20 \times d/20$ were used for discretization (252 nodes). In this case, the parameter δ was below 0.1% with 6 symmetric and antisymmetric modes ($n_S = n_A = 5$) considered for the outer regions.

Due to the symmetry of the problem, the incident S0 (A0) mode generates only symmetric (antisymmetric) modes in both reflected and transmitted fields. Although this fact can be used to considerably reduce the number of Lamb modes to be accounted for in MDM as well as in HFEM, the coefficients of both symmetric and antisymmetric modes up to the same order were retained as unknown variables in the present analysis, which provided a way to validate the solutions by checking if the coefficients of the absent modes in the numerical solution were negligible.

B. S0-mode incidence

For the S0-mode incidence, the computed reflection and transmission coefficients of S0 mode are shown in Fig. 2 as functions of the normalized frequency fd/c_T for different values of $K_N\, d/\mu$ and $K_T\, d/\mu$ for a fixed stiffness ratio $K_T/K_N = 0.4$. In Fig. 2, it is clearly shown that the results by MDM and HFEM are in excellent agreement, indicating the adequacy of the obtained solutions.

Figure 2 shows that for the S0-mode incidence, the transmission coefficient of S0 mode decreases, and the reflection coefficient increases, both monotonically with the frequency. This feature is qualitatively analogous to the reflection/transmission behavior of a bulk longitudinal wave at normal incidence to a spring-type interface between two semi-infinite elastic solids,[4] and will be discussed later. The results for different ratios K_T/K_N with a fixed $K_N\, d/\mu$ are plotted in Fig. 3 by HFEM, and show almost the same curve for different ratios. This indicates that the S0-mode reflection and transmission characteristics are essentially governed by the normal stiffness but not by the tangential one. As clearly shown in Fig. 2, increase of $K_N\, d/\mu$ shifts the $|T_{S0}|$ ($|R_{S0}|$)-frequency curves to higher frequency.

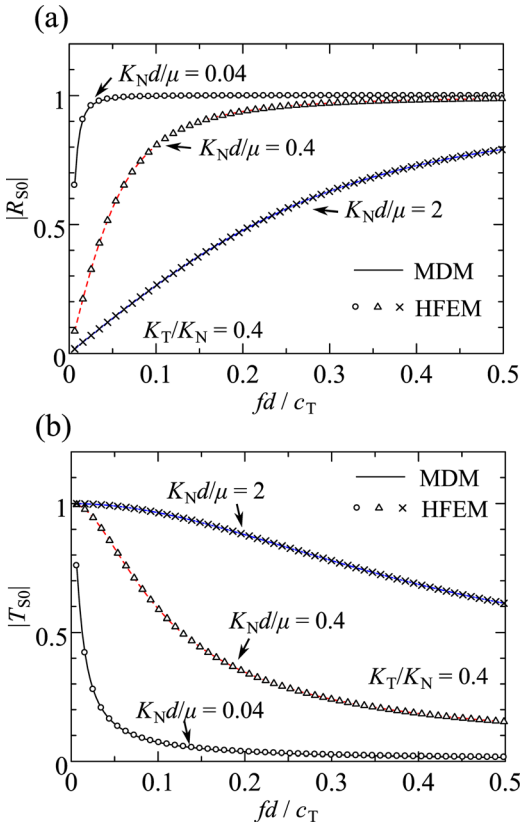

FIG. 2. Variation of the coefficients of the (a) reflected and (b) transmitted S0 mode with the normalized frequency for the S0-mode incidence, for different normalized stiffnesses.

Due to the normalization in Eq. (5), $|R_{S0}|^2$ and $|T_{S0}|^2$ give the time-averaged energy flux of the reflected and transmitted S0 mode along the plates. Correspondingly, $|R_{S0}|$ and $|T_{S0}|$ represent the ratios of their amplitude to those of the incident S0 mode. On the other hand, the time-averaged energy flux is zero for higher-order Lamb modes, and the coefficients $|R_{Sn}|$ and $|T_{Sn}|$ ($n = 1, 2, \ldots$) do not provide direct quantitative meaning. Instead, the ratios of the horizontal displacement amplitude of each mode at $x = 0^{\pm}$, $z = 0$, $|u^R_{Sn}| \equiv |R_{Sn} U^S(0; k^S_{-n})|$ and $|u^T_{Sn}| \equiv |T_{Sn} U^S(0; k^S_{+n})|$, to the corresponding amplitude of the incident S0 mode, $|u^{inc}_{S0}| \equiv |U^S(0; k^S_{+0})|$, are examined to quantify the relative magnitude of higher-order Lamb modes generated at the joint interface. The results for S1 and S2 modes are shown in Fig. 4, which shows that as the frequency increases, the interaction of the incident S0 mode with the interface gives rise to higher-order Lamb modes with higher amplitude, especially for the reflected S1 and S2 modes. For the frequency range considered, however, their relative amplitudes are as small as a few percent, indicating that the conversion into higher-order Lamb modes is not considerable.

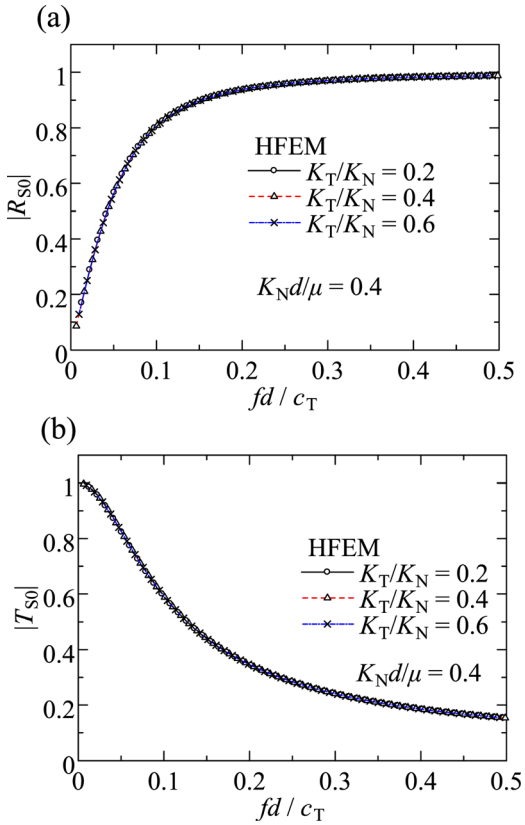

FIG. 3. Variation of the coefficients of the (a) reflected and (b) transmitted S0 mode with the normalized frequency for the S0-mode incidence, for different stiffness ratios.

C. A0-mode incidence

The corresponding reflection and transmission coefficients of A0 modes for the A0-mode incidence are shown in Fig. 5 for the same set of interfacial stiffnesses as in Fig. 2. The two numerical methods give almost identical results in this case, too, although small discrepancy is visible between their results, e.g., for $K_T d/\mu = 0.8$ in Fig. 5(a). In contrast to the S0-mode incidence, Fig. 5 shows that the A0-mode reflection and transmission coefficients vary with frequency in a complicated manner. In particular, there are particular values of $f\ d/c_T$ at which $|T_{A0}| = 1$ ($|R_{A0}| = 0$) or $|T_{A0}| = 0$ ($|R_{A0}| = 1$). Such non-monotonic frequency dependence is not present in the reflection/transmission characteristics of bulk longitudinal or transverse waves at normal incidence to a spring-type interface between semi-infinite solids. The frequency dependence of the reflection and transmission coefficients appears to be governed dominantly by the tangential stiffness K_T but also influenced by the normal stiffness K_N to some extent, since the curves for different ratios K_T/K_N do not overlap in Fig. 6. As a general trend, the increase of K_T shifts the zero points of $|R_{A0}|$ or $|T_{A0}|$ to higher frequencies.

The ratios of the vertical displacement amplitude of each mode at $x = 0^{\pm}$, $z = 0$, $|w^R_{An}| \equiv |R_{An} W^A(0; k^A_{-n})|$ and $|w^T_{An}| \equiv |T_{An} W^A(0; k^A_{+n})|$, to the corresponding amplitude of the incident A0 mode, $|w^{inc}_{A0}| \equiv |W^A(0; k^A_{+0})|$, are shown in Fig. 7 for A1 and A2 modes. It is found that A1 mode is present with significant amplitude, comparable with A0 mode, for a broad range of frequency, while the relative

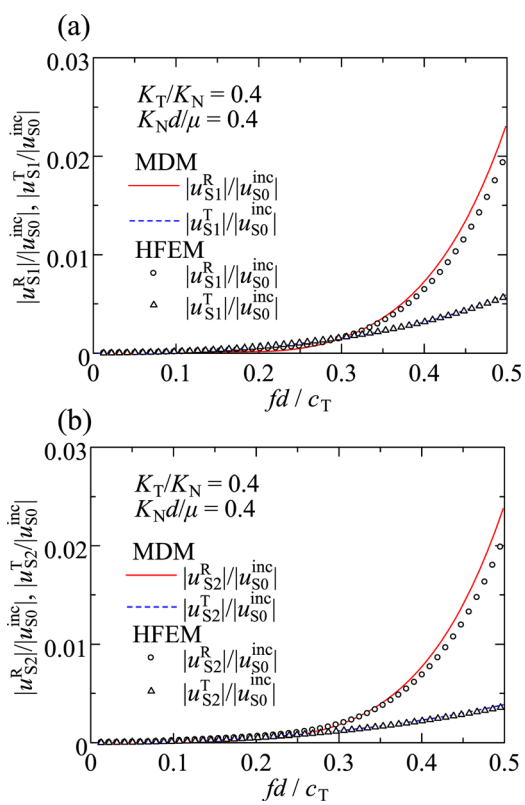

FIG. 4. Variation of the relative displacement amplitude of the reflected and transmitted (a) S1 and (b) S2 modes with the normalized frequency for the S0-mode incidence.

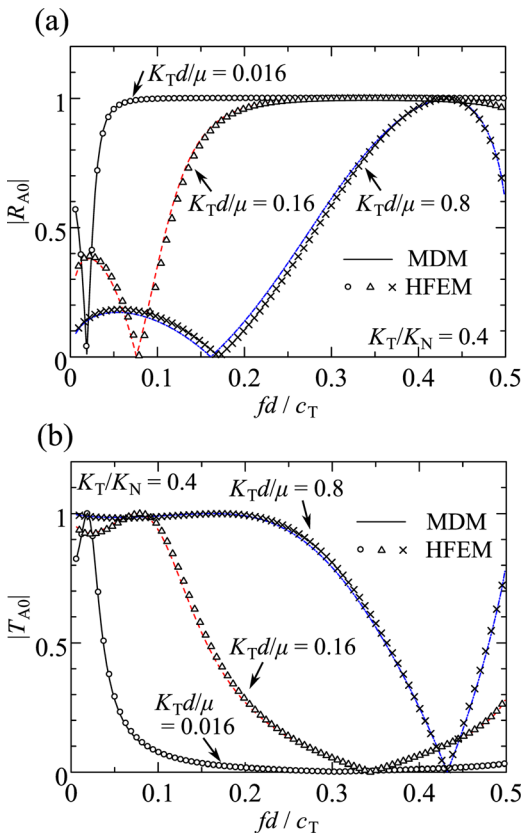

FIG. 5. Variation of the coefficients of the (a) reflected and (b) transmitted A0 mode with the normalized frequency for the A0-mode incidence, for different normalized stiffnesses.

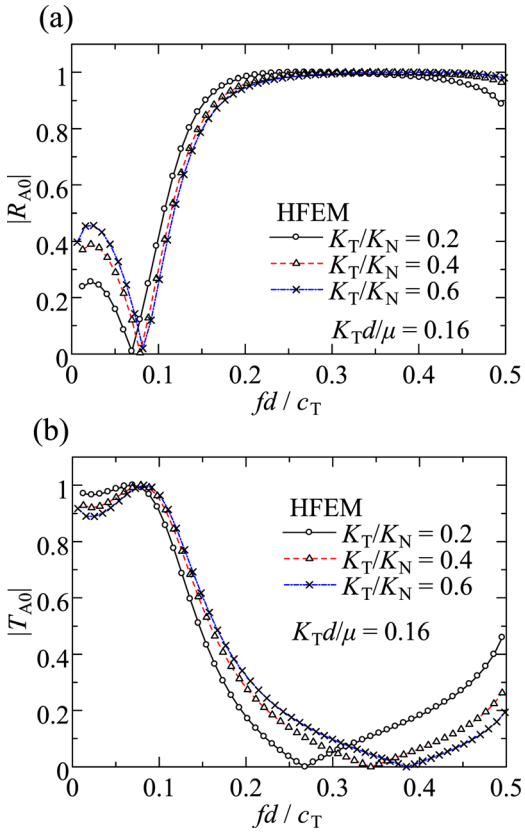

FIG. 6. Variation of the coefficients of the (a) reflected and (b) transmitted A0 mode with the normalized frequency for the A0-mode incidence, for different stiffness ratios.

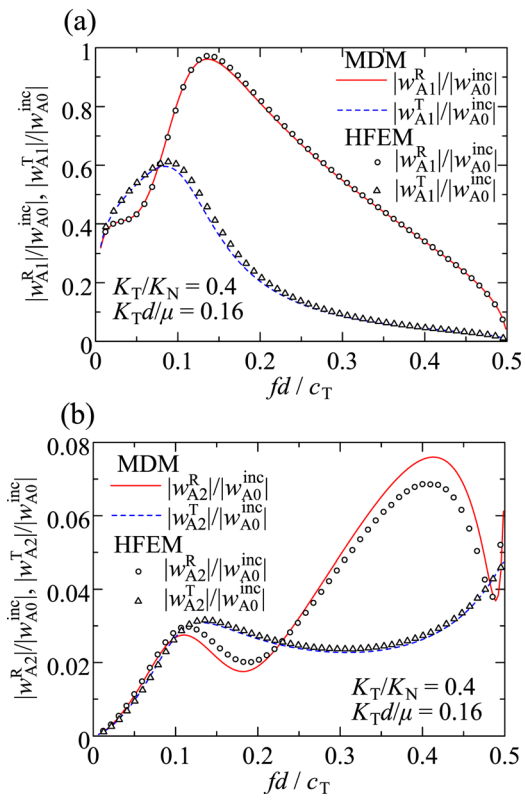

FIG. 7. Variation of the relative displacement amplitude of the reflected and transmitted (a) A1 and (b) A2 modes with the normalized frequency for the A0-mode incidence.

amplitude of A2 mode is typically a few percent. It is noted that the agreement between MDM and HFEM appears less satisfactory for A2 mode as the frequency increases. Accuracy of the solutions by HFEM depends on the choice of parameters such as the interior region size L and the size of finite elements. In addition, it can be pointed out that HFEM is not perfectly suited to calculate the amplitude of high-order modes with high accuracy, since these modes are attenuated to small values at the boundaries of the FEM region. With smaller L, HFEM gives the A2-mode coefficients closer to the results of MDM by employing greater numbers of modes for the outer region and smaller finite element size.

IV. DISCUSSIONS

A. S0-mode incidence

The lowest-order symmetric Lamb mode (S0 mode) accompanies longitudinal motions of a plate dominantly. It then appears intriguing to examine the S0-mode reflection/transmission characteristics in the light of an approximate classical theory for longitudinal wave in thin plates. The longitudinal motion in a sufficiently thin plate obeys a simple wave equation with the velocity

$$c_1 = \sqrt{\frac{E}{(1-\nu^2)\rho}}, \tag{11}$$

where $E = \mu(3\lambda + 2\mu)/(\lambda + \mu)$ is Young's modulus.[40] Note that this is the zero-frequency limit of the phase velocity of S0 mode. When two plates are joined at $x = 0$ and subjected to incident longitudinal wave of unit amplitude, the horizontal displacement in the frequency domain is expressed by

$$u(x) = \begin{cases} \exp(\mathrm{i}kx) + R\exp(-\mathrm{i}kx), & x < 0 \\ T\exp(\mathrm{i}kx), & x > 0 \end{cases} \tag{12}$$

where $k = \omega/c_1$ and R and T are the complex reflection and transmission coefficients. Corresponding to Eq. (2a), the boundary conditions at $x = 0$ are given by

$$\frac{\partial u}{\partial x}(0^+) = \frac{\partial u}{\partial x}(0^-) = \frac{K_N}{\rho {c_1}^2}[u(0^+) - u(0^-)], \tag{13}$$

which determines R and T as functions of a non-dimensional parameter $\rho c_1\omega/K_N$, i.e.,

$$R = \frac{1}{1 + \mathrm{i}\,\dfrac{2K_N}{\rho c_1 \omega}}, \quad T = \frac{\mathrm{i}\,\dfrac{2K_N}{\rho c_1 \omega}}{1 + \mathrm{i}\,\dfrac{2K_N}{\rho c_1 \omega}}. \tag{14}$$

As a matter of fact, these explicit relations are identical to those for bulk longitudinal waves at normal incidence to a spring-type interface between two semi-infinite media,[4] except that c_1 is substituted in place of the bulk longitudinal wave velocity c_L.

From Eq. (14), it is clear that $|R| \to 0$ and $|T| \to 1$ when $\rho c_1\omega/K_N$ approaches zero, while $|R| \to 1$ and $|T| \to 0$ when $\rho c_1\omega/K_N$ becomes infinitely large. A characteristic frequency

is given by $\rho c_1\omega/K_N = 2$ at which $|R| = |T| = 1/\sqrt{2}$, namely, the incident energy is divided equally into reflected and transmitted waves. In Fig. 8, the reflection and transmission coefficients of S0 mode by the Lamb wave analysis are compared to those of the longitudinal wave in the thin-plate model, as functions of the normalized frequency $\rho c_1\omega/K_N$. When normalized in this fashion, the results for S0 mode with different joint stiffnesses appear identical to the predictions of the thin-plate model for a wide range of $\rho c_1\omega/K_N$. This implies that the partial transmission/reflection characteristics of S0 Lamb mode can be well predicted by the corresponding simple thin-plate model. This makes the interpretation of partially transmitted or reflected S0-mode Lamb wave relatively straightforward for nondestructive testing and structural health monitoring. By evaluating the transmission or reflection ratio of S0 mode, one can use Eq. (14) to estimate the normal stiffness of an imperfect joint, which gives information of, e.g., degree of partial closure of a crack in a plate. Recently, Lee and Staszewski[20] discussed the effect of closure of a fatigue crack on its detection when S0-mode Lamb wave was used. By numerical modeling, these authors show that a closed crack exhibits greater transmitted S0-mode amplitudes as compared to an open crack, in qualitative conformity with the present finding.

B. A0-mode incidence

Since A0-mode Lamb wave accompanies flexural motions of a plate, it is also of interest to examine the reflection/transmission characteristics of flexural waves by a classical theory. To this purpose, the Mindlin plate theory is employed, in which the rotary inertia and shear deformation are accounted for.[41] The flexural wave propagation in a thin plate in the x-direction is represented by the vertical displacement w and rotation φ of the mid-plane ($z = 0$), which obey

$$\begin{aligned}\rho d\frac{\partial^2 w}{\partial t^2} &= \kappa\mu d\left(\frac{\partial^2 w}{\partial x^2} + \frac{\partial \varphi}{\partial x}\right),\\ \rho I\frac{\partial^2 \varphi}{\partial t^2} &= D\frac{\partial^2 \varphi}{\partial x^2} - \kappa\mu d\left(\varphi + \frac{\partial w}{\partial x}\right),\end{aligned} \tag{15}$$

where κ is the shear factor and

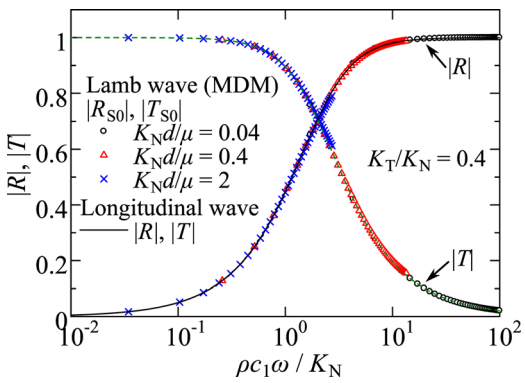

FIG. 8. Variation of the reflection and transmission coefficients of the longitudinal wave in thin plates and S0-mode Lamb wave with the normalized frequency for different normalized stiffnesses.

$$I = \frac{d^3}{12}, \quad D = \frac{Ed^3}{12(1-\nu^2)}. \tag{16}$$

Substituting monochromatic solutions of the form $w = w_0\exp[\mathrm{i}(kx - \omega t)]$, $\varphi = \varphi_0\exp[\mathrm{i}(kx - \omega t)]$ in Eq. (15), the dispersion relation for the Mindlin plate theory is obtained. For the range $fd/c_T < \sqrt{3\kappa}/\pi$, for a given ω there are propagating modes with real wave numbers

$$k = \pm k_1, \quad k_1 = \frac{\omega}{c_1}\sqrt{\frac{1}{2}(P + \sqrt{P^2 + 4Q})}, \tag{17}$$

and non-propagating modes with imaginary wave numbers

$$k = \pm \mathrm{i}k_2, \quad k_2 = \frac{\omega}{c_1}\sqrt{\frac{1}{2}(-P + \sqrt{P^2 + 4Q})}, \tag{18}$$

where

$$P = 1 + \frac{{c_1}^2}{\kappa {c_T}^2}, \quad Q = \frac{{c_1}^2}{\kappa {c_T}^2}\left(\frac{12\kappa {c_T}^2}{\omega^2 d^2} - 1\right). \tag{19}$$

When a flexural wave is incident on a spring-type joint of thin plates, the wave fields are expressed in the frequency domain as

$$w = \begin{cases} \exp(\mathrm{i}k_1 x) + R_0\exp(-\mathrm{i}k_1 x) + R_1\exp(k_2 x), & x < 0 \\ T_0\exp(\mathrm{i}k_1 x) + T_1\exp(-k_2 x), & x > 0 \end{cases} \tag{20}$$

for the displacement, and likewise for the rotation. In the above expression, R_0 and T_0 are the reflection and transmission coefficients of the propagating mode: R_1 and T_1 are the corresponding coefficients for the non-propagating mode.

To obtain the boundary conditions at $x = 0$, an elementary kinematic relation between the horizontal displacement and the rotation $u(x, z) = \varphi z$ is substituted in Eq. (2a), which is multiplied by z and integrated for $-d/2 < z < d/2$ to yield

$$M(0^+) = M(0^-) = IK_N[\varphi(0^+) - \varphi(0^-)], \tag{21}$$

where $M(x) = D\partial\varphi/\partial x$ is the bending moment. Moreover, Eq. (2b) is integrated for $-d/2 < z < d/2$ to give

$$F(0^+) = F(0^-) = K_T d[w(0^+) - w(0^-)], \tag{22}$$

where $F(x) = \kappa\mu d(\varphi + \partial w/\partial x)$ is the shear force. From Eqs. (21) and (22), a set of linear equations for the four coefficients R_0, R_1, T_0, and T_1 are obtained, which can be solved numerically in a straightforward manner.

In Fig. 9, the amplitude reflection and transmission coefficients $|R_0|$ and $|T_0|$ are computed for the shear factor $\kappa = 5/6$ and compared to the A0-mode coefficients $|R_{A0}|$ and $|T_{A0}|$ by the Lamb wave analysis. It is clearly seen that the Mindlin plate model shows reasonable agreement with the Lamb wave analysis in the situation where the plate is sufficiently thin, i.e., for small values of fd/c_T and $K_T d/\mu$. On the other hand, for relatively large $K_T d/\mu$, the Mindlin plate model predictions tend to deviate from the results for A0 mode as

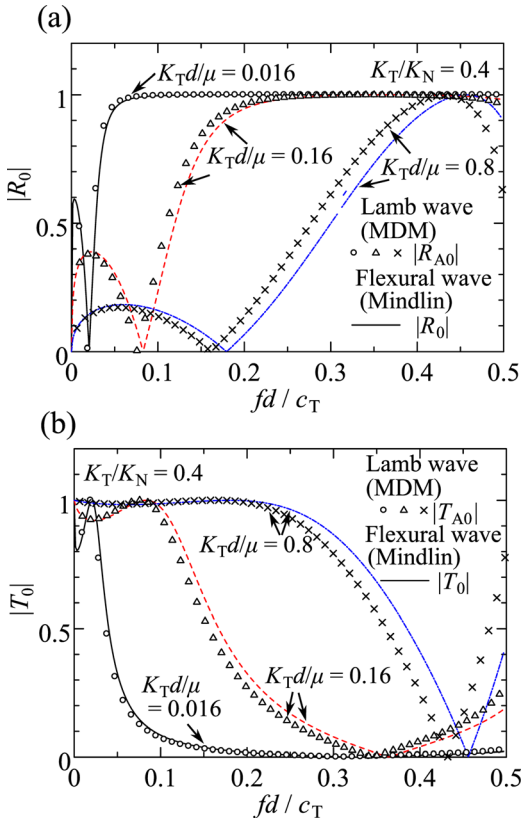

FIG. 9. Variation of (a) the reflection and (b) transmission coefficients of the flexural wave in thin plates (propagating mode) and A0-mode Lamb wave with the normalized frequency for different normalized stiffnesses.

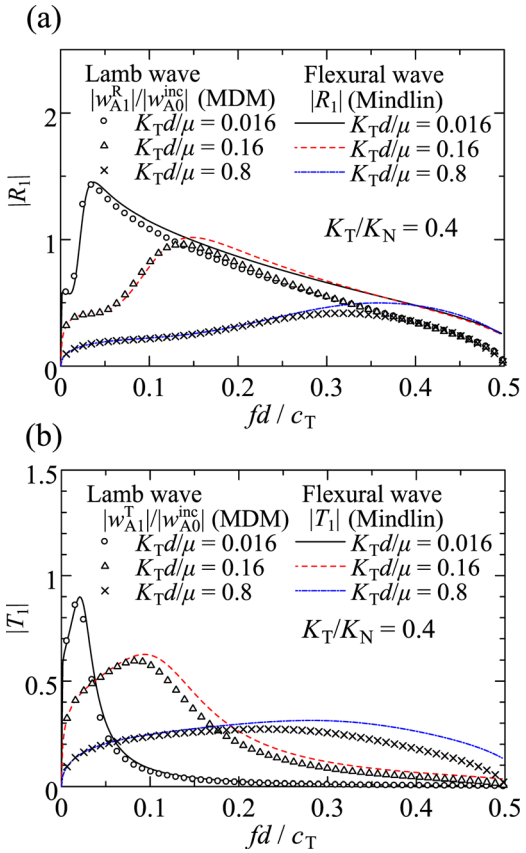

FIG. 10. Variation of the relative displacement amplitudes of the (a) reflection and (b) transmission coefficients of the flexural wave in thin plates (non-propagating mode) and A1-mode Lamb wave with the normalized frequency for different normalized stiffnesses.

fd/c_T increases. The coefficients $|R_1|$ and $|T_1|$ for the non-propagating mode are compared to $|w^R_{A1}|/|w^{inc}_{A0}|$ and $|w^T_{A1}|/|w^{inc}_{A0}|$ for A1 mode in the Lamb wave analysis in Fig. 10. It is found in Fig. 10 that the agreement between the Mindlin plate theory and the Lamb wave analysis is satisfactory when fd/c_T and K_Td/μ are sufficiently small. This indicates that the model based on the Mindlin plate theory is applicable to estimate the relative amplitude of the propagating mode (A0 mode) as well as a non-propagating mode (A1 mode).

As observed in Sec. III C, A0-mode Lamb wave exhibits reflection and transmission characteristics which are frequency-dependent in a complicated manner. Similar features are also seen in the results for the Mindlin plate model. It appears difficult to achieve a simple interpretation of these complicated features, in contrast to the case of S0-mode incidence for which explicit formulae are given in Eq. (14). Although the non-monotonic frequency dependence should be paid due attention, A0-mode Lamb waves can also be used for joint characterization as their theoretical reflection and transmission characteristics can be computed theoretically. Zhang *et al.*[42] discussed an identification procedure for the joint properties of beam waveguides based on a simplistic flexural wave model of the Bernoulli-Euler beam theory. By matching the theoretical reflection or transmission spectrum to the measured one, they estimated the joint properties for beam structures. The results of the present study can be useful to refine such identification procedures based on the full elastodynamic Lamb wave analysis, or the simple model derived above based on the Mindlin plate theory.

C. Influence of interfacial stiffness distribution

In the above discussion, the interfacial stiffnesses have been assumed independent of the thickness coordinate z. In realistic situations, the contact between two plates can be non-uniform and, most probably, weaker at the corners of plate edges. To examine the effect of such inhomogeneous stiffness distributions, numerical simulations are performed assuming the stiffness distributions of the following form:

$$K_T(z) = \gamma K_N(z) = \begin{cases} K_{T0}, & |z| < \phi d/2 \\ K_{T0}\dfrac{1-2|z|/d}{1-\phi}, & \phi d/2 \le |z| \le d/2 \end{cases} \tag{23}$$

where γ is the stiffness ratio and ϕ is a parameter to give the proportion of the thickness of uniform stiffnesses, as illustrated in Fig. 11: K_{N0} and K_{T0} are the stiffnesses for the uniform-stiffness region.

For the S0 and A0 incidence, the reflection and transmission coefficients are plotted in Figs. 12 and 13, respectively, as functions of the normalized frequency for the normalized stiffness $K_{T0}d/\mu = 0.16$ and $\gamma = 0.4$. As seen in Figs. 12 and 13, the characteristic features earlier shown for the joint with uniform stiffness distributions basically remain unchanged even if the interfacial stiffnesses are reduced to

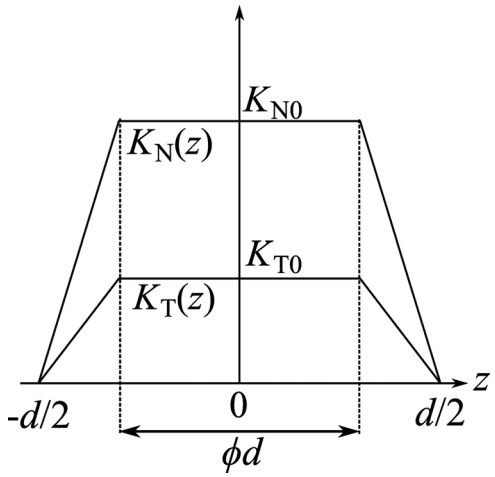

FIG. 11. Assumed distribution of interfacial stiffnesses representing stiffness reduction at corners.

zero at the corners. This was perhaps expected, as both S0 and A0 modes have displacement amplitudes distributed over the whole thickness and not localized near free surfaces. It is noted that this is in some contrast to the case of Rayleigh wave scattering by a surface-breaking crack modeled as a spring-type interface,[19] where the distribution of interfacial stiffness can play a significant role in the Rayleigh wave reflection and transmission as well as conversion into bulk waves.

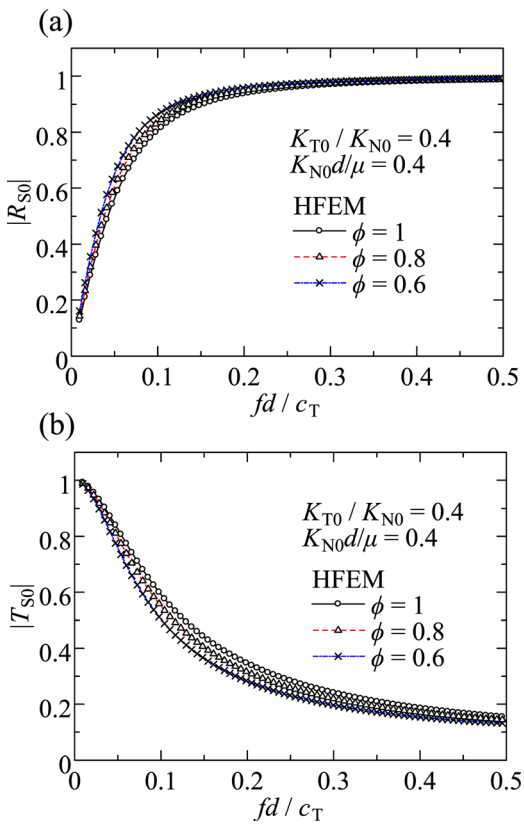

FIG. 12. Influence of the stiffness distribution on the (a) reflection and (b) transmission coefficients of S0 mode, for the S0-mode incidence.

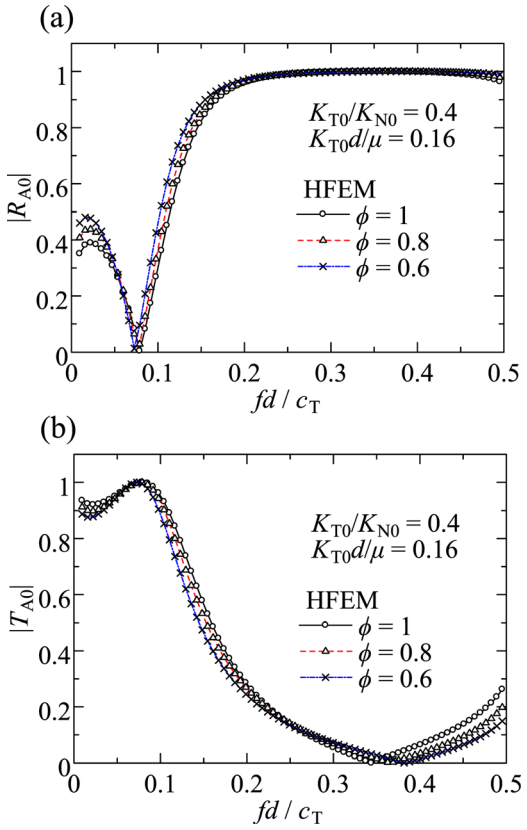

FIG. 13. Influence of the stiffness distribution on the (a) reflection and (b) transmission coefficients of A0 mode, for the A0-mode incidence.

V. CONCLUDING REMARKS

The interaction of low-frequency symmetric and antisymmetric Lamb waves with a spring-type joint of two isotropic plates has been analyzed using the modal decomposition method and the hybrid finite element method. The analysis has elucidated the reflection and transmission characteristics of S0 and A0 mode as functions of the frequency and for different values of joint stiffness. Generation of localized, nonpropagating higher-order Lamb modes has also been demonstrated. The results of the Lamb wave analysis have been compared to those obtained by approximate one-dimensional models constructed employing classical plate theories. As a result, it has been shown that the reflection and transmission characteristics of S0 mode can be accurately reproduced by the model for the longitudinal wave in thin plates, for a wide range of frequency and joint stiffness. Furthermore, the Mindlin plate model for the flexural wave accounting for rotary inertia and shear deformation can well describe the reflection and transmission of A0 mode. The results of the present analysis can be applied to the evaluation of imperfect joint of plates based on measurements of Lamb wave signals. In order to fully appreciate the theoretical findings reported here, corresponding experimental investigations are necessary and constitute a subject of future study. The present analysis has focused on the low-frequency range below the first cut-off frequency where S0 and A0 Lamb waves are the only propagating modes. For higher frequencies, some of higher-order Lamb modes also have the propagating nature, and even the

characteristics for the incidence of the lowest-order modes can be more involved.

[1]R. Clark, W. D. Dover, and L. J. Bond, NDT Int. **20**, 269–275 (1987).
[2]K. Kendall and D. Tabor, Proc. R. Soc. London, Ser. A **323**, 321–340 (1971).
[3]J.-M. Baik and R. B. Thompson, J. Nondestruct. Eval. **4**, 177–196 (1984).
[4]B. W. Drinkwater, R. S. Dwyer-Joyce, and P. Cawley, Proc. R. Soc. London, Ser. A **452**, 2613–2628 (1996).
[5]C. Pecorari, J. Acoust. Soc. Am. **113**, 3065–3072 (2003).
[6]S. Biwa, S. Nakajima, and N. Ohno, Trans. ASME, J. Appl. Mech. **71**, 508–515 (2004).
[7]J.-Y. Kim and J.-S. Lee, J. Appl. Phys. **101**, 043501 (2007).
[8]M. V. Golub and A. Bostrom, Wave Motion **48**, 105–115 (2011).
[9]S. I. Rokhlin and Y. J. Wang, J. Acoust. Soc. Am. **89**, 503–515 (1991).
[10]Y. Lu and J. D. Achenbach, J. Acoust. Soc. Am. **90**, 2576–2585 (1991).
[11]Y. Ishii and S. Biwa, J. Appl. Phys. **111**, 084907 (2012).
[12]J. P. Jones and J. S. Whittier, Trans. ASME, J. Appl. Mech. **34**, 905–909 (1967).
[13]B. Gu, K. T. Nihei, L. R. Myer, and L. J. Pyrak-Nolte, J. Geophys. Res. **101**, 827–835, doi:10.1029/95JB02846 (1996).
[14]S. I. Rokhlin, M. Hefets, and M. Rosen, J. Appl. Phys. **52**, 2847–2851 (1981).
[15]T. Valier-Brasier, T. Dehoux, and B. Audoin, J. Appl. Phys. **112**, 024904 (2012).
[16]B. W. Drinkwater, M.Castaings and B. Hosten, J. Acoust. Soc. Am. **113**, 3161–3170 (2003).
[17]B. Hosten and M. Castaings, J. Acoust. Soc. Am. **117**, 1108–1113 (2005).
[18]Z. L. Li and J. D. Achenbach, Trans. ASME, J. Appl. Mech. **58**, 688–694 (1991).
[19]C. Pecorari, Wave Motion **33**, 259–270 (2001).
[20]B. C. Lee and W. J. Staszewski, IOP Conf. Ser.: Mater. Sci. Eng. **10**, 012059 (2010).
[21]H. Cho and C. J. Lissenden, Struct. Health Monit. **11**, 393–404 (2012).
[22]P. J. Torvik, J. Acoust. Soc. Am. **41**, 346–353 (1967).
[23]R. D. Gregory and I. Gladwell, J. Elast. **13**, 185–206 (1983).
[24]Y. Cho and J. L. Rose, J. Acoust. Soc. Am. **99**, 2097–2109 (1996).
[25]E. Le Clezio, M. V. Predoi, M. Castaings, B. Hosten, and M. Rousseau, Ultrasonics **41**, 25–40 (2003).
[26]D. N. Alleyne and P. Cawley, IEEE Trans. Ultrason. Ferroelectr. Freq. Control **39**, 381–397 (1992).
[27]Y. Cho, D. D. Hongerholt, and J. L. Rose, IEEE Trans. Ultrason. Ferroelectr. Freq. Control **44**, 44–52 (1997).
[28]M. J. S. Lowe and O. Diligent, J. Acoust. Soc. Am. **111**, 64–74 (2002).
[29]M. J. S. Lowe, P. Cawley, J.-Y. Kao, and O. Diligent, J. Acoust. Soc. Am. **112**, 2612–2622 (2002).
[30]M. Castaings, E. Le Crezio, and B. Hosten, J. Acoust. Soc. Am. **112**, 2567–2582 (2002).
[31]A. Gunawan and S. Hirose, J. Acoust. Soc. Am. **115**, 996–1005 (2004).
[32]M. A. Flores-López and R. D. Gregory, J. Acoust. Soc. Am. **119**, 2041–2049 (2006).
[33]B. Kim and Y. Roh, Jpn. J. Appl. Phys., Part 1 **48**, 07GD04 (2009).
[34]A. R. Clough and R. S. Edwards, J. Appl. Phys. **111**, 104906 (2012).
[35]Y. N. Al-Nassar, S. K. Datta, and A. H. Shah, Ultrasonics **29**, 125–132 (1991).
[36]M. V. Predoi and M. Rousseau, Ultrasonics **43**, 551–559 (2005).
[37]M. Koshiba, S. Karakida, and M. Suzuki, IEEE Trans. Sonics Ultrason. **31**, 18–25 (1984).
[38]K. F. Graff, *Wave Motion in Elastic Solids* (Oxford University Press, London, 1975).
[39]J. L. Rose, *Ultrasonic Waves in Solid Media* (Cambridge University Press, Cambridge, 1999).
[40]H. Kolsky, *Stress Waves in Solids* (Dover, New York, 1963).
[41]R. D. Mindlin, Trans. ASME, J. Appl. Mech. **18**, 31–38 (1951).
[42]B. Zhang, T. P. Waters, and B. R. Mace, in *Proceedings of the 2006 SEM Annual Conference and Exposition on Experimental and Applied Mechanics 2006* (Society for Experimental Mechanics, Inc., 2006), Vol. 3, pp. 1409–1416.